Low-noise MEMS vibration sensor for geophysical applications

Article *in* Journal of Microelectromechanical Systems · January 2000

DOI: 10.1109/84.809058 · Source: IEEE Xplore

4 authors, including:

Jonathan Bernstein
Draper Laboratory
66 PUBLICATIONS **1,973** CITATIONS
SEE PROFILE

Raanan Miller
Massachusetts Institute of Technology
66 PUBLICATIONS **3,326** CITATIONS
SEE PROFILE

Low-Noise MEMS Vibration Sensor for Geophysical Applications

Jonathan Bernstein, *Member, IEEE,* Raanan Miller, William Kelley, and Paul Ward, *Member, IEEE*

***Abstract*—The need exists for high-sensitivity, low-noise vibration sensors for various applications, such as geophysical data collection, tracking vehicles, intrusion detectors, and underwater pressure gradient detection. In general, these sensors differ from classical accelerometers in that they require no direct current response, but must have a very low noise floor over a required bandwidth. Theory indicates a capacitive micromachined silicon vibration sensor can have a noise floor on the order of 100 ng/$\sqrt{\text{Hz}}$ over 1-kHz bandwidth, while reducing size and weight tenfold compared to existing magnetic geophones. With early prototypes, we have demonstrated Brownian-limited noise floor at 1.0 μg/$\sqrt{\text{Hz}}$, orders of magnitude more sensitive than surface micromachined devices such as the industry standard ADXL05. [376]**

***Index Terms*— Acceleration measurement, capacitance transducers, geophysical measurements, microelectromechanical devices, micromachining.**

I. Introduction

A VIBRATION sensor can be thought of as a very high-sensitivity accelerometer with no direct current (dc) output requirement. With no drift or bias stability specifications, the design can be optimized to give the lowest noise floor. Applications for these devices include geophysical sensing, machinery vibration and failure prediction, tracking and identification of vehicles or personnel, and underwater pressure gradient sensing.

Traditional vibration sensors using permanent magnets and fine wire coils are called geophones,[1] which measure *velocity* above the fundamental resonance. This is in contrast to capacitive accelerometers that measure *acceleration* below their fundamental resonance. Piezoelectric and ferroelectric accelerometers are also used for these applications. Micromachined sensors can offer size and weight advantages over traditional sensors.

Previous efforts to make micromachined high-resolution vibration sensors or accelerometers have included capacitive [1]–[3], tunneling [4], [5], piezoresistive, optical, and piezoelectric sensors. Capacitive sensors have the advantage of no exotic materials, low noise, and compatibility with CMOS readout electronics. Tunneling sensors have a low noise floor, but due to the small allowable displacement at the tip require a very stiff feedback loop, which reduces the useful bandwidth and dynamic range.

Manuscript received August 8, 1998; revised June 14, 1999. This paper was presented in part at the Transducers Research Foundation Hilton Head Workshop on Solid-State Sensor and Actuators, Hilton Head, SC, 1998. Subject Editor, S. Tabata.

The authors are with the Charles Stark Draper Laboratory, Cambridge, MA 02139-3563 USA

Publisher Item Identifier S 1057-7157(99)09609-2.

[1]Geospace, Inc., GS-14 geophone, Houston, TX 77040 USA.

II. Theory

The sensor is modeled as a spring-mass-damper system with capacitive pickoff. Because no dc output is required, it was decided for initial tests to build a single-capacitor sensor rather than a differential capacitor design. Noise sources modeled include Brownian mechanical noise from air damping and electronic noise from the readout circuit [6].

The Brownian force is $F_B = \sqrt{4kTD}\ (N/\sqrt{\text{Hz}})$ [6], which causes Brownian motion of the proof mass x_B

$$x_B = \frac{\sqrt{4kTD}}{k_{\text{sp}} + j\omega D - \omega^2 M} \qquad \text{m}/\sqrt{\text{Hz}} \tag{1}$$

where D is the damping coefficient of the proof mass M supported by spring constant k_{sp}. Solving for the acceleration which generates the same motion x_B and substituting $Q = \omega_0 M/D$, $\omega_0 = \sqrt{k_{\text{sp}}/M}$, and $g = 9.8$ m/s^2 gives for Brownian equivalent acceleration noise in g/$\sqrt{\text{Hz}}$

$$g_{n,B} = \frac{\sqrt{4kTD}}{Mg} = \frac{1}{g}\sqrt{\frac{4kT\omega_0}{MQ}} \qquad \text{g}/\sqrt{\text{Hz}}. \tag{2}$$

From (2), we see that a large mass and high Q (low damping) are helpful to achieve a low noise floor. To achieve a large mass in a micromachined sensor, one typically uses a wafer-thick proof mass carved from the sensor chip.

In order to use a sensor with a high Q, it must be force-rebalanced to prevent ringing at the resonant frequency. In the work presented here, the sensors are overdamped, with a Q of about 0.3. A vacuum package is typically necessary to achieve very high Q (>10 000).

The sensitivity of the device is calculated for the simple case of a dc bias voltage with a high-input impedance buffer amplifier. A bias voltage of $1/2$ the snap-down voltage (V_{SD}) is assumed. The sensitivity at low frequency (M_0) is the volts/meter in the sense gap times the meters/g of the proof mass well below resonance

$$M_0 = \frac{V_{\text{SD}}}{2x_0}\,\frac{Mg}{k_{\text{sp}}} = \frac{V_{\text{SD}}}{2x_0}\,\frac{g}{\omega_0^2} \qquad \text{V/g}. \tag{3}$$

The snap-down voltage is $V_{\text{SD}} = \sqrt{8k_{\text{sp}}x_0^3/27\varepsilon_0 A}$, where x_0 is the capacitor sense gap and A is the capacitor area.

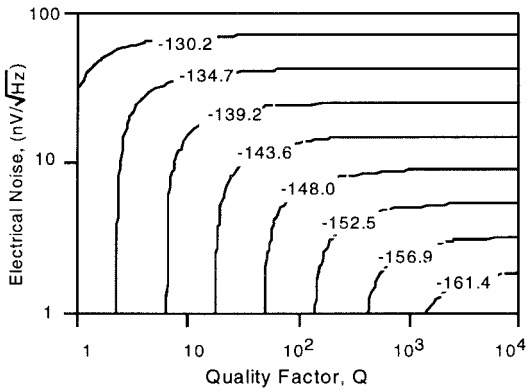

Fig. 1. Total noise in decibels referenced to 1 g/$\sqrt{\text{Hz}}$, as a function of Q and front-end electrical noise.

Substituting for the mass M and V_{SD} gives for sensitivity M_0

$$M_0 = \frac{g}{\omega_0}\sqrt{\frac{2t\rho_{Si}x_0}{27\varepsilon_0}} \qquad \text{V/g} \tag{4}$$

where t is the proof mass thickness, and ρ_{Si} is the density of silicon. From this, we see that sensitivity is inversely proportional to the fundamental resonant frequency.

We consider also an electronic readout noise component, which has (in general) equivalent input current noise and voltage noise components. The total equivalent front-end noise is called $v_{n,e}$. This voltage noise can be converted to an equivalent acceleration noise in g's by dividing by the transducer sensitivity in volts per gram (V/g)

$$g_{n,e} = \frac{v_{n,e}}{M_0} \qquad \text{g}/\sqrt{\text{Hz}}. \tag{5}$$

The total noise is the rms combination of electrical and Brownian contributions

$$g_{n,T} = \sqrt{g_{n,B}^2 + g_{n,e}^2} \qquad \text{g}/\sqrt{\text{Hz}}. \tag{6}$$

Voltage noise for a low-noise CMOS front end is typically in the 5–10-nV/$\sqrt{\text{Hz}}$ range above the $1/f$ corner. Lower noise can be obtained, but at the cost of increased current consumption.

To achieve a noise level of 10 ng, a vacuum package must be used to reduce Brownian motion noise.

Fig. 1 is a contour map of combined g-equivalent noise as a function of electrical noise (1 nV to 100 nV/$\sqrt{\text{Hz}}$) and Q (1 to 10^4). The decibel scale on the map is decibels referenced to 1 g/$\sqrt{\text{Hz}}$, hence 10^{-8}g/ $\sqrt{\text{Hz}}$ corresponds to -160 dB. To achieve a noise level of 10 ng/$\sqrt{\text{Hz}}$ requires a Q of 3000 and a front-end equivalent noise of under 2 nV/$\sqrt{\text{Hz}}$. For this calculation, the silicon proof mass is assumed to be 4 mm $\times$ 4 mm $\times$ 0.38 mm with a resonant frequency of 1 kHz.

Table I lists the design goals for the three resonant frequencies of the fabricated devices.

III. Electronics Design

To evaluate the vibration sensor prototypes, two types of electronics were used: an open-gate JFET source follower and a custom CMOS application-specified integrated circuit (ASIC) fabricated at Orbit Semiconductor.[2] The JFET buffer allowed quick, reasonably low noise measurements to be made with a very compact circuit (inside the sensor package), although $1/f$ and current noise are high at low frequencies. The ASIC uses a carrier to reduce $1/f$ noise, resulting in better low-frequency performance.

TABLE I
Design Goals for Micromachined Vibration Sensor

	Units	500 Hz Sensor	1 kHz Sensor	10 kHz Sensor
Resonant Frequency	Hz	500 Hz	1,000	10 kHz
Self Noise Floor * (Combined Brownian and electronic)	ng/$\sqrt{\text{Hz}}$	25	43	338
Sensitivity with unity gain buffer	V/g	0.49	0.245	0.025
Maximum g-level (open loop)	g's	0.3	1.2	120
Displacement per g	m	10^{-6}	2.5 X 10^{-7}	2.5 X 10^{-9}

* Assumes 8 nV/$\sqrt{\text{Hz}}$ electrical noise, Q = 100

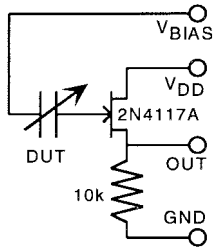

Fig. 2. Open-gate JFET buffer circuit.

Fig. 2 shows the open-gate JFET buffer circuit used. This circuit has a dc input impedance of several teraohms, which combined with a typical sensor capacitance of 50 pF gives an *RC* time constant of several minutes. To speed the approach to the stable bias point, it was sometimes necessary to shine light in the package. The light temporarily increases the JFET leakage current, thereby decreasing the impedance of the gate node. This reset technique is sometimes used with nuclear particle counters to reset a critical node without adding stray capacitance and leakage current.

A custom CMOS mixed signal ASIC was designed in-house and fabricated at Orbit Semiconductor. The design implements synchronous modulation/demodulation using square waves and a novel radio frequency (RF) rebalance technique. The block diagram of the system is shown in Fig. 3. The circuit rebalances the proof mass below the frequency range of interest, while allowing higher frequency vibrations to move the proof mass open-loop.

Equal and opposite 100-kHz square waves are applied to the sensor and a reference capacitor. Vibrations cause a mismatch between the fixed capacitor and the time-varying sensor. The charge amplifier converts the capacitance mismatch into an output voltage which is then amplified by the alternating current (ac) gain stage.

[2] Orbit Semiconductor, Inc., Sunnyvale, CA, USA.

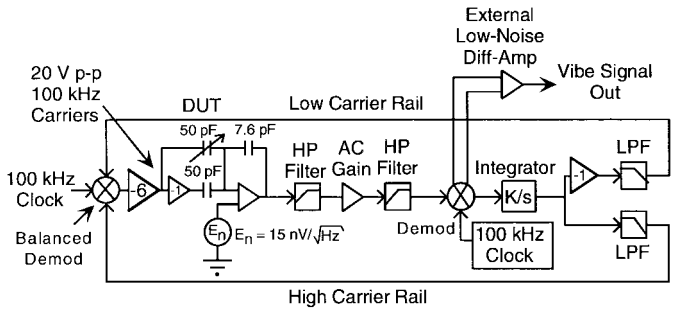

Fig. 3. CMOS ASIC block diagram.

The resulting vibration signal is amplitude modulated on a 100-kHz square wave carrier. The amplifier stages process this signal at 100 kHz to avoid $1/f$ noise in the CMOS transistors. The vibration signal is demodulated after ac amplification to recover the vibration signal. The output of the demodulator is an error signal representing an acceleration or capacitance mismatch between the sensor and the reference capacitor. The high frequency part of this signal is passed to an external low-noise amplifier. The low frequency part is integrated, inverted, and low-pass filtered to create the low and high carrier rails. The difference between the low and high rails represents the low-frequency feedback used to force the sensor capacitance back to the reference capacitor value. The modulator has three inputs, the low and high rails, and the clock signal. The output of this modulator is switched between the high and low rails to create a variable amplitude square wave carrier, which is applied to the sense capacitor. The square wave is inverted to drive the reference capacitor.

Application of ac voltage to the sensor applies a force proportional to the square of the applied voltage amplitude. The integral rebalance controller adjusts the carrier amplitude and tunes the time average sensor capacitance to match the fixed reference capacitor. Under open loop operation, maximum g's are determined when the proof mass moves about 10% of the sense gap. Closed-loop maximum g's are determined by the maximum available rebalance voltage, which is typically limited to some fraction of snap-down voltage.

The bandwidth of the rebalance loop is adjustable and was selected to be low ($<$1 Hz). The rebalance loop nulls dc and sub 1-Hz accelerations maintaining signal null with changes in temperature and sensor orientation. This allows high gain for ac signals and avoids saturation of the 5-V CMOS electronics. Vibrations above 1 Hz are not rebalanced and are sensed open-loop from the demodulator output.

IV. Sensor Fabrication

The sensors are fabricated on 0.38-mm-thick double-side polished wafers using the Bosch process in a surface technology systems (STS) etcher. A recess 3-μm deep is etched into the wafer to define anchors and create the sense gap. 30-μm-deep damping-relief trenches are then etched to reduce squeeze-film damping. A 10-μm-thick boron diffusion is used to create an etch stop layer on both faces of the wafer. After electrostatic bonding to a glass wafer with readout electrodes, the STS etcher is used to trench through the wafer. A brief anisotropic etch then undercuts the springs.

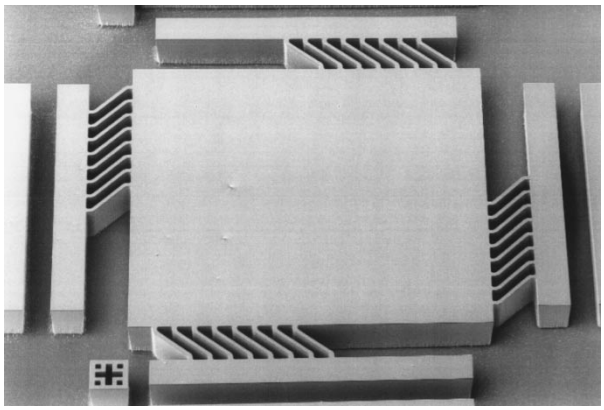

Fig. 4. Vibration sensor structure etched through the wafer (380 μm), before anisotropic etch.

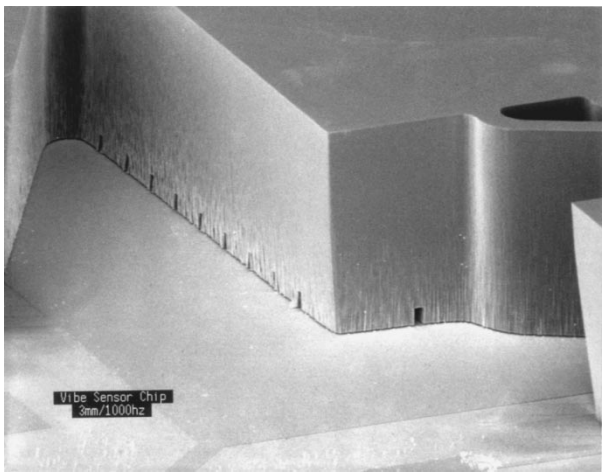

Fig. 5. Corner of device showing electrodes and damping-reduction trenches.

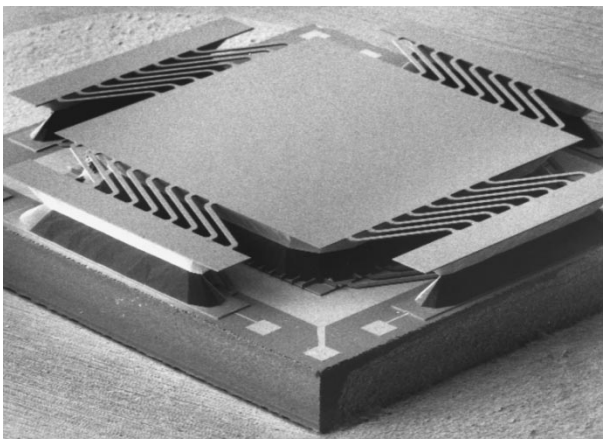

Fig. 6. Vibration sensor after anisotropic etching, leaving thin boron-doped flexures supporting large proof mass.

Figs. 4 and 5 show a sensor chip after the deep inductively coupled plasma etch and before the anisotropic etch. A central proof mass is supported by springs attached to four anchors on a glass substrate. Damping-relief trenches are visible in Fig. 5 facing the glass substrate. Fig. 6 shows a completed prototype sensor.

TABLE II
TEST RESULTS FROM CMOS ASIC/VIBRATION SENSOR INTEGRATION

Sensor Design Bandwidth (Hz)	Proof-Mass Size (mm)	Maximum Carrier Amplitude (V)	Carrier drive level (V P-P)	Delta - Cap. per g (pF/g)	Charge Amp input noise (nV/$\sqrt{Hz}$)	Charge amp gain (V/V)	AC gain (V/V)	Scale Factor (V/g)	g-noise Theor. (g/$\sqrt{Hz}$)	g-noise Measured (g/$\sqrt{Hz}$)
10k	4	100	20	0.02	15	13.86	16.8	0.392	8.9×10^{-6} electrical noise limited	8.40E-06
1K	3	20	20	0.48	15	8.06	1	1.260	400×10^{-9} Brownian noise limited	1.02E-06
500	4	10	10	3.59	15	9.42	1	3.420	200×10^{-9} Brownian noise limited	

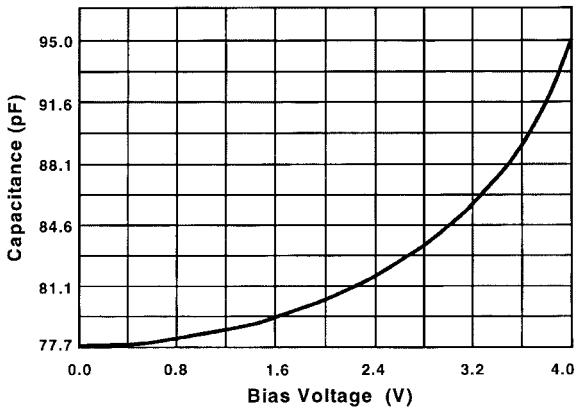

Fig. 7. *CV* curve. Capacitance varies 17 pF (22%) at 4-V bias.

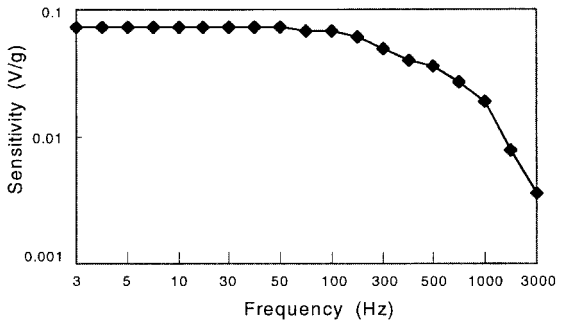

Fig. 8. Frequency response of 3 mm × 3 mm device, design resonance at 1 kHz, $Q = 0.3$.

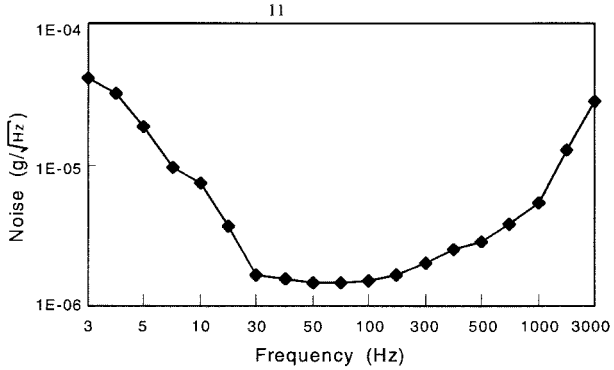

Fig. 9. Plot of acceleration noise in g/$\sqrt{\text{Hz}}$ using source-follower buffer circuit. Device is same as Fig. 8.

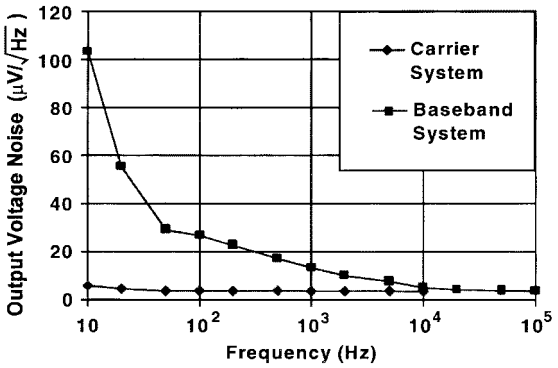

Fig. 10. Baseband versus synchronous modulation/demodulation noise with Orbit CMOS ASIC readout chip.

Devices were designed and fabricated with three proof mass sizes (3 mm^2, 4 mm^2, and 5 mm^2) and three resonant frequencies (500 Hz, 1 kHz, and 10 kHz) to cover various applications. Kovar flat-packs were used to house the sensors with internal (JFET) preamp or external (custom CMOS buffer) readout circuit.

V. TEST RESULTS

Chip level testing includes *capacitance–voltage (CV)* curves (Fig. 7) and current–voltage curves to measure leakage resistance (typically greater than 1 TΩ). Frequency response with the open-gate JFET buffer is shown in Fig. 8. A sensitivity of 42 mV/g was obtained at a bias voltage of 3.7 V. The noise floor (measured on a vibration isolated platform) was 1.5 μg/$\sqrt{\text{Hz}}$ (Fig. 9), limited by Brownian noise for this over-damped device. A battery powered low-noise pre-amp using OP 37 op-amps was necessary to lift the signal level above the noise floor of the HP 3563A dynamic signal analyzer for noise measurements.

Fig. 10 shows the advantage of the RF carrier readout chip over a baseband CMOS readout. Orders of magnitude reduction in $1/f$ noise are achieved at low frequencies using this ASIC.

TABLE III
VIBRATION SENSOR/ACCELEROMETER SURVEY

Manufacturer	Part ID	Band-width	Noise Floor ($\mu g/\sqrt{Hz}$)	Fig. of Merit BW / Noise Floor ($Hz^{3/2}/\mu g$)	Ref.
Draper (Exp. Data)	(experimental)	300 Hz	1.0	300	
Draper (Theoretical)	(experimental)	10 kHz	0.34	29,400	
Analog Devices	ADXL05	4 kHz	600	6.6	Analog Dev. Data book
CSEM[3]	ACSEM02-T/5	1 kHz	40	25	CSEM Product Literature
CSEM	MS 6100	800 Hz	100	8	CSEM Product Literature
Kistler	8363A(X)	150 Hz	24	6.25	K-Beam User's Guide
UCLA LWIM Accel.	(experimental)	50 Hz	0.1	500	LWIM web site
JPL Tunnel Accel.	(experimental)	120 Hz*	0.1	1,200	[5]

* It is difficult to define a bandwidth for this device, since it is used beyond resonance. The proof mass resonant frequency is used here.

Table II summarizes test results using the CMOS ASIC, including electrical noise, ac gain, theoretical noise, and measured noise floor. A noise floor of 1.0 $\mu g/\sqrt{Hz}$ was achieved with a 1-kHz nominal device, limited by Brownian noise. The predicted electrical noise floor was only 0.12 $\mu g/\sqrt{Hz}$ for this device. An electrical noise power spectral density of 0.4 $\mu g/\sqrt{Hz}$ was measured with the bias voltage turned down to zero, which removes the Brownian motion component. The higher measured noise is due to higher than expected damping and electrical voltage noise.

VI. DISCUSSION AND CONCLUSIONS

Table III is a summary of commercial off-the-shelf (COTS) and research vibration sensors about which information was available. For each device, the bandwidth (BW), noise floor (NF), and a figure of merit (FOM) are given (FOM= BW/NF). This FOM is independent of the BW for a given family of capacitive sensors, given constant electrical noise and the relations between BW, sensitivity, and maximum bias voltage (which is a fixed fraction of the snap-down voltage). One can see from the table that the theoretical performance is 30 times better than that of the best experimental devices, which are in turn orders of magnitude better than current COTS devices. One can conclude that future devices will push down the noise floor to well under 0.1 $\mu g/\sqrt{Hz}$ with a 1-kHz sensing bandwidth. At this sensitivity, they could replace geophones in some applications.

In conclusion, a bulk micromachined vibration sensor has been fabricated and tested with a novel, custom CMOS ASIC, which removes $1/f$ noise while requiring only a single sense capacitor and one dummy capacitor. Vibration noise as low as 1.5 $\mu g/\sqrt{Hz}$ was achieved with a JFET buffered sensor and 1 $\mu g/\sqrt{Hz}$ using a custom CMOS ASIC. Theory indicates that orders of magnitude improvements can be made over industry standard COTS sensor in both bandwidth and noise floor by the use of wafer-thick bulk micromachining technology with optimized low-noise electronics. These sensors will be useful for geophysical work, machinery monitoring, and sensing of vehicles and people.

[3] Centre Suisse d'Electronique et de Microtechnique SA (CSEM).

ACKNOWLEDGMENT

The authors would like to thank the Charles Stark Draper Laboratory for supporting this work.

REFERENCES

[1] W. Henrion, L. DiSanza, M. Ip, S. Terry, and H. Jerman, "Wide dynamic range direct digital accelerometer," in *Tech. Dig. 1990 Solid-State Sensor and Actuator Workshop*, Hilton Head Island, SC, June 4–7, 1990, pp. 153–157.

[2] K. Bult, A. Burstein, and D. Chang, "Wireless integrated microsensors," in *Proc. 1996 Hilton Head Solid State Sensor and Actuator Conf.*, 1996, pp. 205–210.

[3] M. Lemkin *et al.*, "A 3-axis force balanced accelerometer using a single proof mass," in *Proc. 9th Int. Conf. Solid-State Sensors and Actuators-Transducers '97*, Chicago IL, June 1977, pp. 1185–1188.

[4] C. H. Liu, J. D. Grade, A. M. Barzilai, K. K. Reynolds, A. Partridge, J. J. K. Rockstad, and T. W. Kenney, "Characterization of a highly sensitive tunneling accelerometer," in *Transducers '97 Tech. Dig.*, 1997, pp. 471–472, paper 2B3.07.

[5] H. K. Rockalnd, T. W. Kenny, P. Kelley, and T. Gabrielson, "A micro-fabricated electron-tunneling accelerometer as a directional underwater acoustic sensor," in *Proc. Acoustic Particle Velocity Sensors: Design, Performance, and Applications*, 1996, pp. 57–68.

[6] T. B. Gabrielson, "Mechanical-thermal noise in micromachined acoustic and vibration sensors," *IEEE Trans. Electron Devices*, vol. 40, pp. 903–909.

Jonathan Bernstein (S'80–M'82) received the B.S.E.E. degree with honors in engineering-physics from Princeton University, Princeton, NJ, and the M.S.E.E. and Ph.D. degrees from the University of California at Berkeley. In addition, he received National Science Foundation and Hertz Foundation graduate fellowships.

Currently, he is with the Charles Stark Draper Laboratory, Cambridge, MA, as the Task Leader for micromechanical acoustic sensors (hydrophones, microphone, and vibration sensors), accelerometers, and advanced micromachined tuning-fork gyroscopes, in which capacity he has designed, analyzed, and fabricated these transducers. He is responsible for the process development for silicon monolithic sensors, including single crystal silicon, polysilicon, PZT-on-Si, and electroformed metal microstructures. He has also carried out process development to combine on-chip JFET circuitry with these micromechanical sensors and PZT-on-Silicon technology.

Dr. Bernstein has received Draper's Distinguished Performance Award, Best Invention Award (twice), and Best Publication Award.

Raanan Miller received the Ph.D. degree in electrical engineering from the California Institute of Technology (Caltech), Pasadena, CA, in 1997

Currently, he is with the Charles Stark Draper Laboratory, Cambridge, MA, as a Senior Member of the Technical Staff in the micromechanical group. He is involved in process development for next-generation MEMS gyroscopes and accelerometers. In addition, he has designed, fabricated, and tested a micromachined field asymmetric ion mobility (FAIM) spectrometer for chemical warfare agent detection.

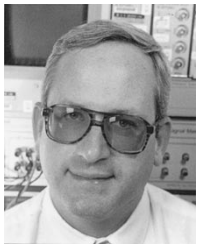

William Kelley received the B.S.E.E. degree (*cum laude*) from Northeastern University, Boston, MA, in 1991

Currently, he is with the Charles Stark Draper Laboratory, Cambridge, MA, as a Senior Engineer in the microelectronics group. He is the co-creator on two patents: RF Balanced Capacitive Vibration Sensor System and Micromechanical Pressure Gauge having Extended Sensor Range.

Mr. Kelley has received two Draper awards as a member of the ASIC design team for First-Pass Success. In addition, he has received an Outstanding Performance Award for contributions to the development of the micromechanical gyro.

Paul Ward (S'83–M'85) received the B.S. and M.S. degrees in electrical engineering from Northeastern University, Boston, MA.

In 1985, he joined the Charles Stark Draper Laboratory, Cambridge, MA, where he is currently a Principal Engineer and Microelectronics Group Leader. He is the principal engineer for Draper's micromachined gyroscope and accelerometer electronics, including application-specific integrated circuits (ASIC's). He has been the principal electrical engineer for many challenging projects, including ppm-level radiation test systems, electron-spin and nuclear-magnetic resonance precision signal references, resonator and interferometer fiber-optic gyroscopes, and most recently, micromechanical instrument electronics. He holds 11 U.S. patents, has many patents pending, and has co-authored numerous papers.

Mr. Ward is a member of Eta Kappa Nu and ARRL. He received the 1994 Draper Distinguished Performance Award along with others for their work on the micromechanical gyroscope and electronics and the 1997 Draper Distinguished Performance Award for his work on a commercially viable yaw rate sensor instrument. In addition, he has received numerous Draper Recognition Awards, as well as the 1996, 1997, and 1998 Best Technical Patent Awards.